Biophysical Journal, Volume *115*

Supplemental Information

Nanoscale Topography and Poroelastic Properties of Model Tissue Breast Gland Basement Membranes

Gloria Fabris, Alessandro Lucantonio, Nico Hampe, Erik Noetzel, Bernd Hoffmann, Antonio DeSimone, and Rudolf Merkel

SUPPORTING MATERIAL
Nanoscale topography and poroelastic properties of model tissue breast gland basement membranes

G. Fabris[1,3], A. Lucantonio[2], N. Hampe[1], E. Noetzel[1], B. Hoffmann[1], A. DeSimone[2], and R. Merkel[1,*]

[1]Institute of Complex Systems, ICS-7: Biomechanics, Forschungszentrum Jülich, Jülich, Germany
[2]International School for Advanced Studies - SISSA, Trieste, Italy
[3]Dept. of Mechanical Engineering, Stevens Institute of Technology, Hoboken, NJ, USA
[*]Correspondence: r.merkel@fz-juelich.de

1 COMPUTATIONAL MODEL OF THE MEMBRANE INDENTATION

We model the basement membrane as a polymer-based, non-linear poroelastic material that we describe using the theory for swelling gels developed in (1). In the following, we briefly summarize the governing equations, along with the boundary conditions and the numerical formulation of the model.

1.1 Governing equations and boundary conditions

The displacement of the membrane's polymer network with respect to a reference configuration $\mathcal{B}$ is described by the vector field $\mathbf{u}$. This field describes the state of the membrane together with the solvent concentration c per unit reference volume. The solvent within the membrane (in this case, water) is additionally characterized by a chemical potential μ, which quantifies the energy it carries. The driving force of solvent migration is given by the gradient of the chemical potential. The corresponding solvent molar flux $\mathbf{h}$ (units $\mathrm{mol}/\mathrm{m}^2 \cdot \mathrm{s}$) characterizes the relative motion of the solvent with respect to the polymer matrix. We will use the symbol $\mathbf{F} = \mathbf{I} + \nabla\mathbf{u}$ (with $\mathbf{I}$ the identity) for the deformation gradient and write $J = \det\mathbf{F}$ for its determinant, and $\mathbf{F}^\star = J\mathbf{F}^{-T}$ for its cofactor.

Swelling processes are governed by the equations of balance of forces and moments that, assuming inertia negligible, read:

$$\operatorname{div}\mathbf{S} = 0\,, \qquad \operatorname{skw}\mathbf{S}\mathbf{F}^{\mathrm{T}} = 0\,, \tag{1}$$

where $\mathbf{S}$ denotes the first Piola-Kirchhoff stress tensor, and by the balance of solvent mass:

$$\dot{c} = -\operatorname{div}\mathbf{h}\,, \tag{2}$$

subject to the initial condition $c = c_\mathrm{o}$. Here, $c_\mathrm{o} = (J_\mathrm{o} - 1)/(\Omega J_\mathrm{o})$ is the solvent concentration per unit reference volume initially present within the membrane in its equilibrium state, with J_o the volume ratio between the reference and the dry configuration and Ω the solvent molar volume. The coupling between Eqs. 1-2 occurs both at the kinematic and at the constitutive levels.

From the viewpoint of kinematic coupling, the polymer matrix and the solvent are considered to be separately incompressible; hence, the change in volume of the membrane is related to the change in solvent concentration:

$$J = 1 + \Omega(c - c_\mathrm{o})\,. \tag{3}$$

This constraint is enforced through the Lagrange multiplier p.

As concerns the constitutive equations, we prescribe the following Flory-Rehner representation for the free energy density of the membrane (1, 2):

$$\psi(\mathbf{F}, c) = \psi_\mathrm{e}(\mathbf{F}) + \psi_\mathrm{m}(c)\,, \tag{4}$$

where

$$\psi_\mathrm{e}(\mathbf{F}) = \frac{G_\mathrm{d}}{2J_\mathrm{o}}(J_\mathrm{o}^{1/3}\mathbf{F}\cdot\mathbf{F} - 3) \quad \text{and} \quad \psi_\mathrm{m}(c) = \mathcal{R}Tc\left[\log\left(\frac{\Omega J_\mathrm{o}c}{1+\Omega J_\mathrm{o}c}\right) + \chi\frac{1}{1+\Omega J_\mathrm{o}c}\right] \tag{5}$$

are the neo-Hookean elastic energy of the polymer network and the Flory-Huggins free energy of solvent-polymer mixing, respectively. Here, G_d is the shear modulus of the dry polymer, $\mathcal{R}$ is the universal gas constant, T is the absolute temperature of

the environment, and χ is the polymer-solvent mixing parameter. For the consistency with thermodynamical principles, the corresponding constitutive equations are given by:

$$\mathbf{S} = \frac{\partial \psi_{\mathrm{e}}}{\partial \mathbf{F}} - p\mathbf{F}^{\star}\,, \quad \mu = \frac{\partial \psi_{\mathrm{m}}}{\partial c} + \Omega p\,, \quad \mathbf{h} = -\frac{c\,D}{\mathcal{R}T}\nabla\mu\,, \tag{6}$$

where D is the diffusivity of the solvent within the membrane. Here, we have chosen a Darcy-like law to relate the water flux to the gradient of chemical potential. The value of the model parameters used in the simulations are reported in Table S1.

In the reference configuration, because of the chemical equilibrium, the membrane's chemical potential μ_{o} is homogeneous and equals that of the external solvent. Specifically, we consider an external solvent in equilibrium with its vapor, so that $\mu_{\mathrm{o}} = \mu_{\mathrm{e}} = 0$ J/mol. Moreover, the reference configuration is stress-free, hence it is identified by the conditions $\mathbf{F} = \mathbf{I}$, $\mu = \mu_{\mathrm{o}}$ and $\mathbf{S} = 0$, which together determine the swelling ratio J_{o} as the solution of the equation:

$$\log\left(1 - \frac{1}{J_{\mathrm{o}}}\right) + \frac{1}{J_{\mathrm{o}}} + \frac{\chi}{J_{\mathrm{o}}^2} + \frac{G_{\mathrm{d}}\Omega}{\mathcal{R}T}\frac{1}{J_{\mathrm{o}}^{1/3}} = 0\,, \tag{7}$$

which coincides with Eq. 6 of the main text upon introducing the initial water volume fraction $\phi_{\mathrm{o}} = 1 - 1/J_{\mathrm{o}}$. As fitting parameters for model calibration, we choose λ_{o}, χ and D. In particular, once λ_{o} and χ are known, the incremental shear modulus $G = G_{\mathrm{d}}/J_{\mathrm{o}}^{1/3}$ with respect to the reference configuration can be readily computed from:

$$G = -\frac{\mathcal{R}T}{\Omega}\left[\log\phi_{\mathrm{o}} + 1 - \phi_{\mathrm{o}} + \chi(1-\phi_{\mathrm{o}})^2\right]\,, \tag{8}$$

while the incremental bulk modulus K obtained by linearizing the constitutive equations is (3):

$$K = -\frac{G}{3} + \frac{\mathcal{R}T}{\Omega}\left(\frac{1}{\phi_{\mathrm{o}}} - 2\chi\right)(1-\phi_{\mathrm{o}})^2\,. \tag{9}$$

For symmetry reasons, 1/4 of the membrane was chosen as the computational domain (see Fig. 6b in the main text); the corresponding zero normal displacement and zero normal solvent-flux boundary conditions were imposed on the symmetry planes. The substrate was assumed to be rigid, frictionless, and impermeable, which amounts to prescribing zero normal displacement and zero normal solvent flux on the bottom surface of the membrane. Apart from the boundaries in contact with the substrate and the indenter, the free surface of the membrane was assumed to be in chemical equilibrium with the surrounding water bath at all times, *i.e.* $\mu = \mu_{\mathrm{e}}$.

The indentation procedure was modeled as follows. Starting from the equilibrium state of free swelling with $\mu = \mu_{\mathrm{o}}$, the indenter was vertically displaced at constant speed $v = 50\,\mu$m/s and brought into contact with the membrane, until the indentation depth δ as measured experimentally was reached. The indenter was modeled as a rigid body. A penalty formulation was employed to describe frictionless contact between the membrane and the spherical indenter, *i.e.* the normal contact pressure $p_c = -kd$ for $d \le 0$ ($p_{\mathrm{c}} = 0$ for $d > 0$) was applied on the contact region $\mathcal{S}_{\mathrm{c}}$ of the membrane surface, with k the penalty factor and d the distance between the surface of the indenter and the top surface of the membrane.

1.2 Weak form of the governing equations and numerical procedures

In order to solve the problem set in the previous paragraphs by means of the finite element method, we recast the governing equations 1_1, 2, and 3 in weak form. Then, the weak formulation of the problem reads: find $\mathbf{u}$, c, p and g such that the following equations

$$\int_{\mathcal{B}} \mathbf{S}\cdot\nabla\tilde{\mathbf{u}} = \int_{\mathcal{S}_{\mathrm{c}}} \mathbf{s}\cdot\tilde{\mathbf{u}}\,, \qquad \int_{\mathcal{B}} (-\dot{c}\tilde{\mu} + \mathbf{h}\cdot\nabla\tilde{\mu}) - \int_{\mathcal{S}_{\mathrm{f}}} (g\,\tilde{\mu}) = 0\,, \tag{10}$$

$$\int_{\mathcal{B}} (J - 1 - \Omega c + \Omega c_{\mathrm{o}})\,\tilde{p} = 0\,, \qquad \int_{\mathcal{S}_{\mathrm{f}}} (\mu(c,p) - \mu_{\mathrm{e}})\,\tilde{g} = 0\,, \tag{11}$$

hold for arbitrary test fields (indicated with a superposed tilde) compatible with the Dirichlet boundary conditions. Here, $\mathbf{s} = -p_{\mathrm{c}}\mathbf{n}$ is the contact traction, with $\mathbf{n}$ the outward unit normal to the *current* contact surface $\mathcal{S}_{\mathrm{c}}$, and g is the Lagrange multiplier enforcing the chemical equilibrium on the free surface $\mathcal{S}_{\mathrm{f}}$ of the membrane. The weak form of the governing equations is complemented by the constitutive relations 6. Equations 10-11 and the corresponding boundary conditions were implemented

Table S1: Parameter values used in the numerical simulations.

Parameter	*Value*	*Description*
h	$(160-450)\,\mathrm{nm}$[a]	Membrane thickness
L	$100h$	Membrane in-plane length
λ_o	$4.2-5$[b]	Initial swelling stretch of the membrane
χ	$0.42-0.48$[b]	Solvent-polymer mixing parameter
D	$(0.01-1.5)\times10^{-7}\,\mathrm{m^2/s}$[b]	Solvent diffusivity
Ω	$1.8\times10^{-5}\,\mathrm{m^3/mol}$	Solvent molar volume
T	$298\,\mathrm{K}$	Ambient temperature
r	$0.5, 3.5\,\mu\mathrm{m}$	Indenter radius
v	$50\,\mu\mathrm{m/s}$	Indentation speed
δ	$(90-180)\,\mathrm{nm}$[a]	Indentation depth

a. Variable. Value selected according to experiment.

b. Fitting parameter.

into the finite element software COMSOL Multiphysics v5.2a using the Weak Form PDE mode (see (4) for details regarding the solvers). Specifically, quadratic shape functions were used for $\mathbf{u}$, c and g, while the pressure field p was discretized using linear shape functions to get a reliable approximation of the volume constraint. The implicit, variable-order (from 1 to 5), adaptive step-size BDF solver was used for time-stepping. A quasi-Newton algorithm was employed to solve iteratively the non-linear algebraic system resulting from the finite element discretization at each time step. The direct solver MUMPS was chosen for the solution of the linearized algebraic system at each iteration. The mesh consisted of triangular elements for the surface of the indenter, and of prism and hexahedra for the membrane, corresponding to a total of about 4×10^4 degrees of freedom. Local mesh refinement over the contact area between the indenter and the membrane was performed to ensure convergence and accuracy of the solution.

For given values of the model parameters, the solution of equations 10-11 allows to evaluate the indentation force, *i.e.* the integral of the contact traction over $\mathcal{S}_\mathrm{c}$, as a function of time. This was then compared with the experiments to calibrate the model parameters λ_o, D and χ. In particular, a least-square fitting procedure was employed for such a calibration. The cost functional, *i.e.* the squared distance between the numerical and experimental force-time curves, exhibits several local minima, which correspond to different sets of optimal fitting parameters. To ensure that the global minimizer was found in the optimization procedure, after a preliminary sampling of the parameter space, the range of the fitting parameters was restricted, and the optimization was performed multiple times starting from 100 randomly generated points within such range. In each optimization run, the gradient-free BOBYQA optimization algorithm was employed to perform the least-square fitting. After completing the optimization runs, the minimizer corresponding to the lowest value of the cost function was selected.

2 FORCE-RELAXATION CURVES: COMPARISON BETWEEN EXPERIMENTAL DATA AND NUMERICAL RESULTS

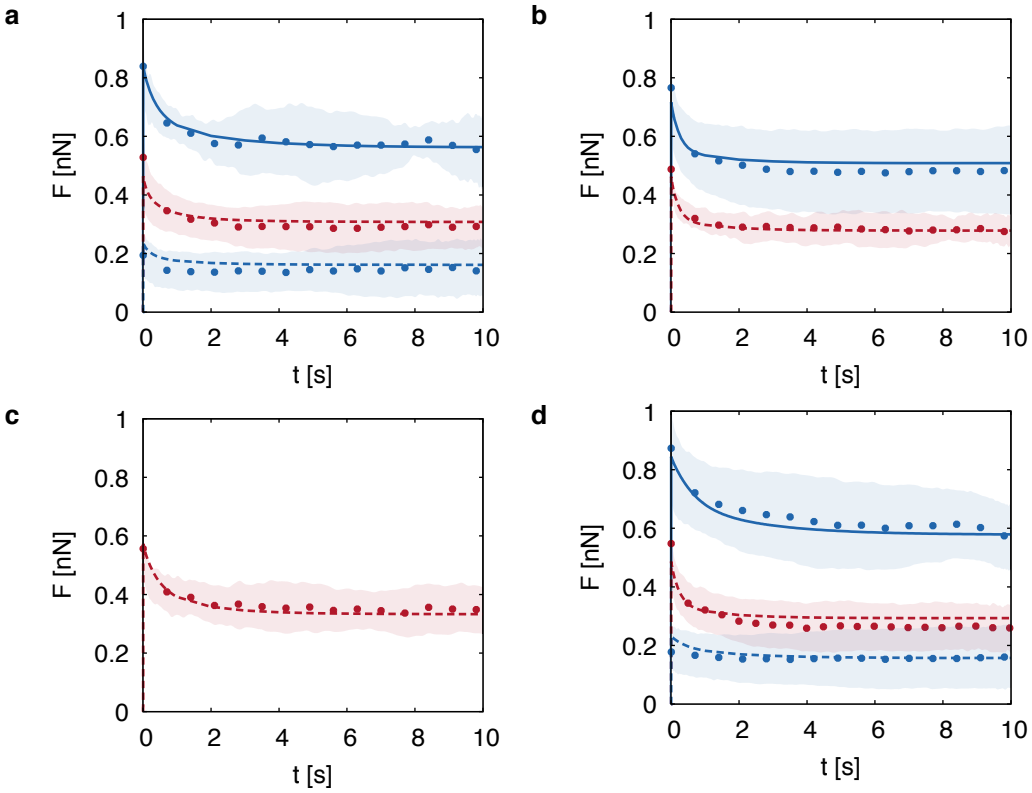

Figure S1: Force-relaxation curves: comparison between experimental (dots) and numerical (lines) results for four different membranes (a-d) and for different values of both indenter radius R: 3.5 µm (blue), 0.5 µm (red), and force setpoint F: 1 nN (solid lines), 0.5 nN (dashed lines). Dots and shaded areas correspond to the spatial averages and the standard deviations of the indentation force, respectively, as computed from experimental data.

3 EFFECT OF WATER PRESSURE ON MEMBRANE PERMEABILITY

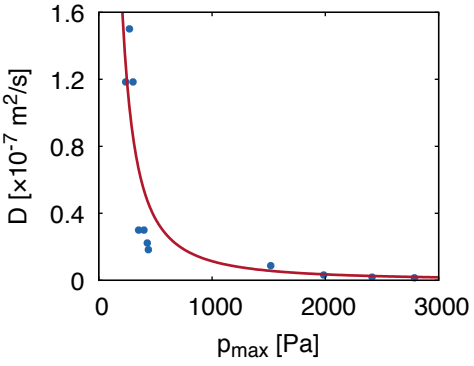

Figure S2: Water diffusivity as a function of the maximum water pressure in the membrane recorded during each indentation test. Dots represent data from numerical simulations. The red line is a power-law fit to the data: $0.0013 \cdot p_{\max}^{-1.686}$.

4 EFFECT OF OSCILLATING COMPRESSIVE BODY LOAD ON SOLVENT FLUX AND MEMBRANE VOLUME

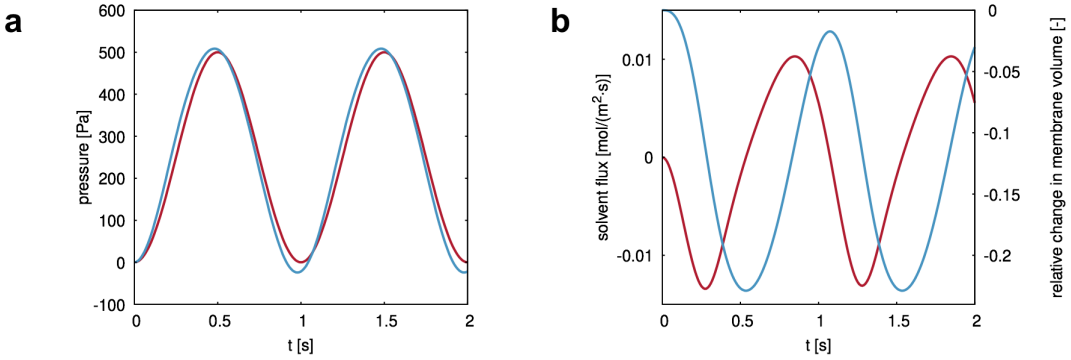

Figure S3: (a) Solvent pressure within (red curve) and outside (blue curve) the membrane. (b) Surface-averaged solvent flux (red curve, negative values meaning outward flux) computed on the boundary of the membrane in contact with the external solvent. Relative volume change of the membrane (blue curve): $\int_{\mathcal{B}} \Omega(c - c_{\mathrm{o}})\,\mathrm{d}V / \int_{\mathcal{B}} \mathrm{d}V$

.

In this simulation, a membrane with thickness $L = 300$ nm is subject to an oscillating compressive body load $-(p_e(t)/L)\mathbf{e}_3$, $p_e(t) = p_{\max}/2[1 - \cos(2\pi f t)]$, in the direction $\mathbf{e}_3$ of the thickness, with peak pressure magnitude $p_{\max} = 500$ Pa and frequency $f = 1$ Hz. This body load mimics inertia loads associated to suckling during lactation (5, 6). The geometry and boundary conditions are taken as for indentation simulations (except for the contact with the indenter, which is here absent); the other model parameters are chosen as $\lambda_{\mathrm{o}} = 4.6$, $\chi = 0.488$, $D = 7.5 \times 10^{-8}\mathrm{m}^2/\mathrm{s}$, which correspond to a typical membrane in our indentation experiments. The external fluid pressure (red curve in Fig. S3a) is supposed to vary according to p_e, so that applied traction on the top surface of the membrane is $-p_e\mathbf{e}_3$ and the external chemical potential is $\mu_{\mathrm{e}} = \Omega p_{\mathrm{e}}$. As reported in Fig. S3a, the volume-averaged fluid pressure μ/Ω within the membrane (blue curve) closely follows the time course of the external pressure, with a slightly different period due to the non-equilibrium in solvent transport and a greater amplitude, which drives solvent exchange with the exterior. Such an exchange may be quantified by evaluating the surface-averaged solvent flux (Fig. S3b, red curve, negative values meaning outward flux), which reaches a peak absolute value of 1×10^{-2} mol/m$^2 \cdot$ s. In particular, in the first half of a period (approximately) the membrane expels fluid due to the overpressure developing as a consequence of the compressive body load; the expelled fluid is then mostly regained in the second half of the period, when the average inner pressure is lower than the external pressure. The relative volume change of the membrane, *i.e.*, the ratio between the volume of fluid exchanged with the exterior and the initial volume of the membrane, is depicted in Fig. S3b (blue curve) and reaches a maximum of 22%.

SUPPORTING REFERENCES

1. Lucantonio A., P. Nardinocchi, and L. Teresi. 2013. Transient analysis of swelling-induced large deformations in polymer gels, J. Mech. Phys. Solids 61:205–218.

2. Doi M. 2009. Gel dynamics, J. Phys. Soc. Jpn. 78(5), 052,001

3. Lucantonio A., and P. Nardinocchi. 2012. Reduced models of swelling-induced bending of gel bars, Int. J. Solids Struct. 49:1399–1405.

4. COMSOL Multiphysics Reference Manual, version 5.2a, COMSOL Inc., URL www.comsol.com

5. Ellendorff F., and D. Schams. 1998. Characteristics of milk ejection, associated intramammary pressure changes and oxytocin release in the mare, J. Endocr. 119 219–227

6. Kent J., L. Kennaugh, and P.E. Hartmann. 2003. Intramammary pressure in the lactating sow in response to oxytocin and during natural milk ejections throughout lactation, J. Dairy Res. 70:131–138.